

# Membrane Probe Distribution Heterogeneity: A Resonance Energy Transfer Study

Luís M. S. Loura,<sup>†,‡</sup> Aleksandre Fedorov,<sup>†,§</sup> and Manuel Prieto<sup>\*,†</sup>

*Centro de Química-Física Molecular, Instituto Superior Técnico, P-1049-001 Lisboa, Portugal, and  
Departamento de Química, Universidade de Évora, Rua Romão Ramalho, 59, P-7000-671 Évora, Portugal*

*Received: January 20, 2000; In Final Form: April 17, 2000*

Probe distribution heterogeneity was studied in model membranes (large unilamellar vesicles of dipalmitoylphosphatidylcholine) using resonance energy transfer. Two Förster pairs were used: octadecylrhodamine B (ORB; donor)/1,1',3,3,3',3'-hexamethylindotricarbocyanine (DiIC<sub>1</sub>(7); acceptor) and *N*-(7-nitrobenz-2-oxa-1,3-diazol-4-yl)-dipalmitoylphosphatidylethanolamine (NBD-PE; donor)/*N*-(lissamine-rhodamine B)-dipalmitoylphosphatidylethanolamine (Rh-PE; acceptor). The donors' fluorescence decays were analyzed in the framework of the mean local concentration model (see preceding article). As acceptor concentration distributions, discrete, Gaussian, and sum of two Gaussian functions were considered. In the fluid phase (50 °C), for moderate (<1%) acceptor concentrations, both donors and acceptors of the two pairs are essentially randomly distributed, and the recovered acceptor concentration distribution curves are well described by single narrow Gaussians. For the gel phase (25 °C), a sum of two Gaussians acceptor concentration distribution is necessary to describe the data. It is concluded that, in the gel phase, for the ORB/DiIC<sub>1</sub>(7) pair, acceptors partially segregate into a pseudo (defect) phase and donors are randomly dispersed in the bulk lattice. At variance, for the NBD-PE/Rh-PE pair, partial segregation of both probes into a pseudo (defect) phase occurs at 25 °C. These conclusions are supported by detailed additional photophysical measurements for these probes in membranes (steady-state energy transfer, fluorescence self-quenching in steady and transient states, and energy migration), and agree with the preceding article's simulations.

## 1. Introduction

The study of lateral heterogeneity in membranes is a very relevant area in biophysics, as the occurrence of domains of different compositions seems to be related to specialized membrane functions.<sup>1</sup> Different size scales of domains can be recognized. Large-scale domains (>0.1 μm) can be directly visualized by microscopic techniques.<sup>2,3</sup> Other techniques such as calorimetry<sup>4,5</sup> are useful regarding the study of nonideality of lipid mixtures, but do not give information about small domains. These are best studied by spectroscopic techniques, such as infrared spectroscopy,<sup>6</sup> electron spin resonance spectroscopy,<sup>2,7</sup> and several photophysical approaches. Regarding the latter, the use of fluorescence intensity, lifetimes, anisotropy, and spectra of membrane probes was reviewed recently.<sup>8</sup> Fluorescence recovery after photobleaching (FRAP), together with Monte Carlo simulations, is useful to probe domain sizes and shapes from the decrease in the diffusion coefficient in gel/fluid heterogeneous membranes due to obstruction caused by the gel phase domains.<sup>9,10</sup>

In the preceding article,<sup>11</sup> we showed that due to its strong intermolecular distance dependence (and therefore sensitivity to the degree of heterogeneity of spatial distribution), resonance energy transfer (ET), and in particular the method of the mean local concentration, with recovery of sum-of-two-Gaussians acceptor concentration distributions, can be used semiquantitatively in the detection and study of chromophore distribution

heterogeneity in planar systems. In this work, we apply the acceptor concentration distribution formalism to both the octadecylrhodamine B (ORB)/1,1',3,3,3',3'-hexamethylindotricarbocyanine (DiIC<sub>1</sub>(7)) and *N*-(7-nitrobenz-2-oxa-1,3-diazol-4-yl)-dipalmitoylphosphatidylethanolamine (NBD-PE)/*N*-(lissamine-rhodamine B)-dipalmitoylphosphatidylethanolamine (Rh-PE) donor/acceptor pairs in dipalmitoylphosphatidylcholine (DPPC) large unilamellar vesicles (LUV).

For ORB/DiIC<sub>1</sub>(7), being the fluid phase system almost ideal on terms of probe distribution homogeneity,<sup>12</sup> the main purpose is to understand better the gel phase system and why the classic two-dimensional, discrete concentration formalism does not work.

The pair NBD-PE/Rh-PE has been widely used in biochemical and biophysical studies, such as membrane fusion,<sup>13</sup> asymmetric distribution of probes in the membrane leaflets,<sup>14</sup> intermembrane lipid transfer processes,<sup>15,16</sup> and bilayer phase transition mechanism.<sup>17</sup> The number of reported ET works using this pair is now in the hundreds, making it the most popular choice for ET studies in membranes. In these works ET was merely used as a tool to measure the kinetics of processes that happen in a second or minute time range, and the actual ET kinetics was not object of study. It is of major importance to establish whether this pair is suitable, from the standpoint of homogeneity of distribution of probes, for ET measurements, or on the other hand, if other probes should be considered for the effect.

Two studies involving ET from NBD-PE to an ensemble of Rh-PE acceptors have been recently reported, both in model membranes. Duportail et al.<sup>18</sup> used a random fractal walk formalism to rationalize their results. An approach based on a diffusion-controlled type of interaction is, however, totally inappropriate, as the Förster radius for this pair is quite significant

\* Corresponding author. Address: Centro de Química-Física Molecular, Instituto Superior Técnico, P-1049-001 Lisboa, Portugal. Fax: +351 218464455. E-mail: prieto@alfa.ist.utl.pt.

<sup>†</sup> Centro de Química-Física Molecular, Instituto Superior Técnico, P-1049-001 Lisboa, Portugal.

<sup>‡</sup> Departamento de Química, Universidade de Évora, Rua Romão Ramalho, 59, P-7000-671 Évora, Portugal.

<sup>§</sup> On leave from the Vavilov Optical Institute, St. Petersburg, Russia.

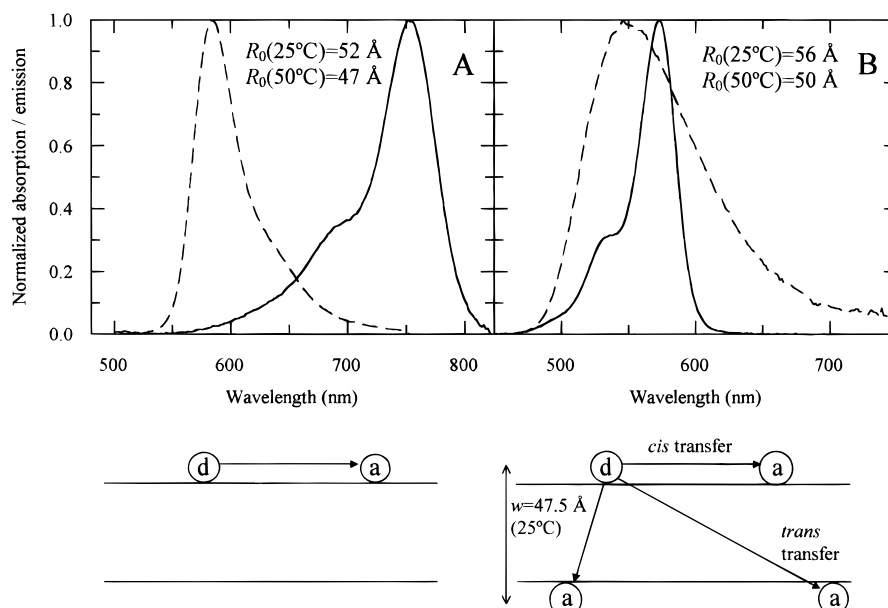


**Figure 1.** Normalized acceptor absorption (solid line) and corrected donor emission spectra (dashed line) in DPPC LUV for the studied ET pairs (top) and schematic representation (d: donor, a: acceptor) of the systems' geometries (bottom; A: ORB/DiIC<sub>1</sub>(7), planar geometry. B: NBD-PE/Rh-PE, bilayer geometry).

(see Results), and translational diffusion is negligible in the time scale of ET, i.e., the system is effectively static. A quantitative ET kinetics study has been performed in fluid phase vesicles of dioleoylphosphatidylcholine (DOPC).<sup>19</sup> The results indicate that the pair is well behaved (regarding randomness of distribution of probes), namely, the linearity of the  $c$  parameter versus acceptor density plot, used by the authors to obtain the average area per lipid. However, a few points were not fully addressed. Steady-state and integrated time-resolved transfer efficiencies are different (unlike, for instance, for the ORB/DiIC<sub>1</sub>(7) pair<sup>12</sup>). On the other hand, the criteria of the goodness of decay data fitting are omitted. Furthermore, as shown in the preceding article, even acceptable statistical parameters could hide a moderate heterogeneity. The ET kinetics of this pair in gel phase vesicles, to our knowledge, has not been addressed, and this is a matter of great importance, regarding the recent use of the pair in the study of the phase transition mechanism.<sup>17</sup> It should be particularly interesting to verify if head-labeled phospholipids, which are widely assumed to disperse randomly in the lipid matrix, obey the predicted random distribution ET kinetics both in the gel phase and in the fluid phase. We expect that the method of acceptor concentration distribution recovery based on the mean local concentration assumption,<sup>20</sup> which has not been used in biochemical or biophysical studies, can help answer these questions.

In addition to the ET studies, other fluorescence measurements (such as fluorescence anisotropy to monitor energy migration, and fluorescence self-quenching of the probes) were also carried out in order to complement the heterotransfer information (see Results).

## 2. Theory

A detailed theoretical discussion of the method is given in the preceding article. Therefore, here we only present the essentials of the formalism. The ET decay curve in a bilayer system with heterogeneity of probe distribution and two different donor lifetime components is described by<sup>11</sup>

$$i_{\text{DA}}(t) = \int_{c_{\text{min}}}^{c_{\text{max}}} f(c) [\exp(-t/\tau_1) + q \exp(-t/\tau_2)] \rho_c(t, c) \rho_t(t, c) dc \quad (1)$$

where the subscripts  $c$  and  $t$  refer to transfer either within the same plane ( $c$ , cis) or to the opposite plane ( $t$ , trans; see Figure 1).  $c$  is proportional to the local concentration of acceptors, and is given by<sup>12</sup>

$$c = \Gamma(2/3) n_{2A} \pi \langle R_0 \rangle^2 \bar{\tau}^{-1/3} \quad (2)$$

$\Gamma$  being the complete gamma function,  $n_{2A}$  the local density of acceptors, and  $\langle R_0 \rangle$  and  $\bar{\tau}$  are the averaged (over the two components) Förster radius and lifetime in the absence of acceptor, respectively.  $f(c)$  is the distribution function for the  $c$  parameter. In this article, we analyze our data assuming the following types of distributions: delta functions centered at some value of  $c$  (in this case we have the usual discrete concentration formalism, here named D), or Gaussian-type distributions:

$$f(c) = A (\exp(-(c - c_1)^2/(2\sigma_1^2)) + h \exp(-(c - c_2)^2/(2\sigma_2^2))) \quad (3)$$

Here  $c_1$  and  $c_2$  are the mean values of each Gaussian,  $\sigma_1$  and  $\sigma_2$  their respective standard deviations, and the  $h$  the ratio of their heights. We considered both single-Gaussian curves (with  $h = 0$ ; formalism 1G) or sum-of-two-Gaussian curves (formalism 2G). As expected, and shown in the preceding article, the latter formalism is the most adequate for dealing with heterogeneous samples, but cases in which the distribution is more homogeneous are described equally well by the simpler formalisms.

The actual ET decay functions for each donor (see eq 1) are given below:

$$\rho_c(t, c) = \exp(-ct^{1/3}) \quad (4)$$

$$\rho_t(t, c) = \exp\left\{-\frac{2c}{\Gamma(2/3)b} \int_0^1 [1 - \exp(-tb^3\alpha^6)] \alpha^{-3} d\alpha\right\} \quad (5)$$

where  $b = (R_0/w)^2 \tau^{-1/3}$ ,  $w$  being the distance between the plane

of donors in one leaflet and the plane of the acceptors in the opposite leaflet. For a planar geometry,  $\rho_i(t, c) = 1$ .

### 3. Materials and Methods

**Experimental Discussion.** In the first system, ORB was used as donor and DiIC<sub>1</sub>(7) was used as acceptor, and in the other system, NBD-PE was used as donor and Rh-PE was used as acceptor. ORB and DiIC<sub>1</sub>(7) were purchased from Molecular Probes (Eugene, OR), and NBD-PE, Rh-PE, and DPPC were obtained from Avanti Polar Lipids (Birmingham, AL). All materials were used as received. LUV of DPPC (ca. 1 mM) in buffer (tris-HCl 50 mM, NaCl 50 mM, EDTA 0.2 mM, pH = 7.4) were prepared by extrusion of lipid dispersions through 100-nm pore diameter polycarbonate membranes.<sup>21</sup> For the NBD-PE/Rh-PE pair, incorporation of both probes by injection of small volumes of ethanol stock solution was found ineffective. The slow, incomplete incorporation of NBD-PE into vesicles has been reported in the literature.<sup>22</sup> For Rh-PE, we found that incubation at 50 °C for a week was insufficient for incorporation (the steady-state fluorescence intensity was about one-third of that of vesicles prepared by cosolubilization of Rh-PE and DPPC). In this way, for this pair adequate amounts of probe solutions in methanol were added to stock solution of DPPC before the evaporation step. Therefore, the probes are distributed in a bilayer geometry for this pair (see Figure 1; we assume that the distribution is symmetrical around the two bilayer leaflets). For the ORB/DiIC<sub>1</sub>(7) pair, adequate small volumes of donor and acceptor solutions in methanol were added to the lipid dispersions. In this case, incorporation of both probes (monitored from fluorescence intensity) was complete in an hour, and the geometry for this pair is planar (see Figure 1), as flip-flop of this probes is negligible if the measurements are carried out within a few hours of preparation of the samples.<sup>12</sup> The ratios ORB:DPPC and NBD-PE:DPPC were approximately 1:10000 and 1:1000, respectively, so that donor excitation energy migration, which would bias the heterotransfer experiments, is negligible. The DiIC<sub>1</sub>(7):DPPC ratio was varied between 1:900 and 1:120 and the Rh-PE:DPPC ratio was varied between 1:500 and 1:80, to get adequate acceptor surface concentrations. In the homotransfer studies, the ORB:DPPC, NBD-PE:DPPC and Rh-PE:DPPC ratios were varied between 1:1800 and 1:300, 1:1000 and 1:30, and 1:5000 and 1:60, respectively. The final lipid concentration was determined by phosphorus analysis.<sup>23</sup> Probe concentrations were calculated using molar absorption coefficients in ethanol ( $\epsilon$ (ORB, 555 nm) =  $85 \times 10^3 \text{ M}^{-1} \text{ cm}^{-1}$ ,<sup>24</sup>  $\epsilon$ (DiIC<sub>1</sub>(7), 741 nm) =  $215 \times 10^3 \text{ M}^{-1} \text{ cm}^{-1}$ <sup>25</sup>) or methanol ( $\epsilon$ (NBD-PE, 463 nm) =  $21 \times 10^3 \text{ M}^{-1} \text{ cm}^{-1}$  and  $\epsilon$ (Rh-PE, 560 nm) =  $95 \times 10^3 \text{ M}^{-1} \text{ cm}^{-1}$ <sup>26</sup>).

**Instrumentation.** Fluorescence decay measurements were carried out with a time-correlated single-photon counting system. The instrumental setup for the ORB/DiIC<sub>1</sub>(7) pair is described elsewhere.<sup>12</sup> In brief, for excitation at 300 nm, a frequency doubled, cavity dumped (3.7 MHz repetition rate), dye laser of Rhodamine 6G (Coherent 701-2), synchronously pumped by a mode-locked Ar<sup>+</sup> laser (514.5 nm, Coherent Innova 400-10) was used. Two filters (Corion LG-400 and LS-650) were added to a Jobin-Yvon HR320 monochromator, to respectively further screen scattered excitation light, and to isolate donor fluorescence from that of acceptor. The emission wavelength was 585 nm, and for the detection, a Hamamatsu R-2809 MCP photomultiplier was used. For the pair NBD-PE/Rh-PE pair, the same instrument was used, and the dye used for excitation of donor at 340 nm was 4-Dicyanomethylene-2-methyl-6-(*p*-dimethylaminostyryl)-4H-pyran (DCM). The emission wave-

length was now 520 nm, and filters added were Corion LG-400 and Corion LS-550. Emission was detected at the magic angle relative to the vertically polarized excitation beam. The number of counts on the peak channel was 20000, and the number of channels per curve used for analysis was 1000, with 44.1 ps/ch for the gel phase experiment (25 °C), and 22.1 ps/ch for the fluid phase experiment (50 °C). Data analysis was carried out with nonlinear, least-squares iterative convolution software based on the Marquardt algorithm<sup>27</sup> using global analysis, i.e., in each case, several decay curves, obtained with different acceptor concentrations, were analyzed together, with linkage of lifetimes and preexponential factors ratio.<sup>12,28</sup> The goodness of the fit was judged from the individual experiments' chi-square values ( $\chi^2$ ), global chi-square value ( $\chi_G^2$ ), and weighted residuals and autocorrelation plots.

Fluorescence steady-state measurements were carried out in the system described by Loura et al.<sup>12</sup> NBD-PE fluorescence intensities were measured at 467 nm excitation and 520 nm emission wavelengths, respectively, with both emission and excitation spectral bandwidths of 4.5 nm. Emission was detected at the magic angle relative to the vertically polarized excitation light. Fluorescence steady-state intensities were corrected for inner filter effects.<sup>29</sup> Absorption spectra were carried out in a Jasco V-560 spectrophotometer. Corrections for turbidity were performed according to Castanho et al.<sup>30</sup>

For evaluation of the critical radius of ET,  $R_0$ , a rewritten Förster's formula was used:<sup>31</sup>

$$R_0 = 0.2108[\kappa^2 \Phi_D n^{-4} \int_0^\infty I(\lambda) \epsilon(\lambda) \lambda^4 d\lambda]^{1/6} \quad (6)$$

where  $R_0$  is expressed in Å units,  $\kappa^2$  is the orientation factor,  $\Phi_D$  is the donor quantum yield in the absence of acceptor,  $n$  is the refractive index of the medium,  $I(\lambda)$  is the normalized donor emission spectrum, and  $\epsilon(\lambda)$  is the acceptor molar absorption coefficient in  $\text{M}^{-1} \text{ cm}^{-1}$  units. Wavelength is expressed in nm units. Unless noted, the value  $\kappa^2 = 2/3$  (corresponding to a dynamic isotropic regime) was assumed, and  $n = 1.33$  was considered. NBD-PE quantum yield in DPPC vesicles was taken as 0.32 at 25 °C.<sup>32,33</sup> On the basis of this value, we determined  $\Phi_D = 0.16$  at 50 °C. For the probes' molar absorption coefficients in vesicles, we determined  $\epsilon_{\text{max}}$  (Rh-PE, 573 nm) =  $88 \times 10^3 \text{ M}^{-1} \text{ cm}^{-1}$  and  $\epsilon_{\text{max}}$  (NBD-PE, 468 nm) =  $20 \times 10^3 \text{ M}^{-1} \text{ cm}^{-1}$ , these values being similar to those in methanol.<sup>26</sup>

The steady-state anisotropy  $\langle r \rangle$  was calculated from<sup>34</sup>

$$\langle r \rangle = (I_{\text{VV}} - GI_{\text{VH}})/(I_{\text{VV}} + 2GI_{\text{VH}}) \quad (7)$$

where the different intensities are the steady-state vertical and horizontal components of the fluorescence emission with excitation vertical ( $I_{\text{VV}}$  and  $I_{\text{VH}}$ , respectively) and horizontal ( $I_{\text{HV}}$  and  $I_{\text{HH}}$ , respectively) to the emission axis. The latter pair of components is used to calculate the  $G$  factor ( $G = I_{\text{HV}}/I_{\text{HH}}$ ).<sup>35</sup>

For surface concentration determination, values of 52.3 and 72.1 Å<sup>2</sup> were assumed for the DPPC polar head areas in the  $L_\beta$  and  $L_\alpha$  phases, respectively.<sup>36</sup> Only half of the lipid molecules (outer monolayer) were considered for this purpose for ORB/DiIC<sub>1</sub>(7); for NBD-PE/Rh-PE, all lipid molecules were taken into account. The bilayer width was taken as 44 Å at 25 °C and 34 Å at 50 °C.<sup>36</sup> To calculate the separation of opposite donor and acceptor planes  $w$  (Figure 1), we added to each of these values 3.5 or 7 Å for the NBD-PE/Rh-PE and Rh-PE/Rh-PE pairs, respectively, to account for the distance from the interface at which the chromophore group of Rh-PE is located



(in the water region).<sup>37</sup> The NBD group in NBD-PE was considered as being at the interphase level.<sup>38</sup>

#### 4. Results

##### Photophysical Properties of the Probes in DPPC Vesicles.

The basic photophysics of the ORB/DiIC<sub>1</sub>(7) pair has been discussed elsewhere.<sup>12</sup> ORB shows a biexponential decay in DPPC vesicles, at both 25 °C ( $\tau_1 = 0.66$  ns,  $A_1 = 0.24$ ,  $\tau_2 = 2.89$  ns,  $A_2 = 0.76$ ) and 50 °C ( $\tau_1 = 0.54$  ns,  $A_1 = 0.18$ ,  $\tau_2 = 1.51$  ns,  $A_2 = 0.82$ ). The relevant  $R_0$  values for the ORB/DiIC<sub>1</sub>(7) pair have also been determined (52.2 Å at 25 °C, 46.8 Å at 50 °C; see Figure 1).

Both NBD-PE and Rh-PE show biexponential decays in DPPC vesicles. We measured for NBD-PE  $\tau_1 = 4.73$  ns ( $A_1 = 0.38$ ),  $\tau_2 = 12.37$  ns ( $A_2 = 0.62$ ) at 25 °C and  $\tau_1 = 0.87$  ns ( $A_1 = 0.25$ ),  $\tau_2 = 6.61$  ns ( $A_2 = 0.75$ ) at 50 °C. These values agree with those of Duportail et al.<sup>18</sup> for NBD-PE in dipalmitoylphosphatidylglycerol ( $\tau_1 = 6.0$  ns ( $A_1 = 0.42$ ),  $\tau_2 = 12.6$  ns ( $A_2 = 0.58$ ) at 20 °C and  $\tau_1 = 1.7$  ns ( $A_1 = 0.06$ ),  $\tau_2 = 5.6$  ns ( $A_2 = 0.94$ ) at 50 °C). For Rh-PE, we measured  $\tau_1 = 3.01$  ns ( $A_1 = 0.88$ ),  $\tau_2 = 5.91$  ns ( $A_2 = 0.12$ ) at 25 °C and  $\tau_1 = 1.81$  ns ( $A_1 = 0.91$ ),  $\tau_2 = 3.00$  ns ( $A_2 = 0.09$ ) at 50 °C. These values agree with those of Medhage et al.<sup>37</sup> in DOPC ( $\tau = 3.0$  ns at 25 °C and  $\tau = 1.8$  ns at 50 °C), who, however, report monoexponential decays. The source of our results' minor long-lived component is not entirely clear, though probably reflects a slight microenvironmental heterogeneity. Note that the pre-exponential factor associated to that component is small for both cases.

Figure 1 shows the emission and absorption spectra for NBD-PE and Rh-PE in DPPC vesicles. Red shifts ( $\lambda_{\text{max,abs}}(\text{NBD-PE}) = 468$  nm,  $\lambda_{\text{max,emi}}(\text{NBD-PE}) = 545$  nm,  $\lambda_{\text{max,abs}}(\text{Rh-PE}) = 573$  nm,  $\lambda_{\text{max,emi}}(\text{Rh-PE}) = 590$  nm) are observed when the maxima values are compared to those in methanol ( $\lambda_{\text{max,abs}}(\text{NBD-PE}) = 463$  nm,  $\lambda_{\text{max,emi}}(\text{NBD-PE}) = 536$  nm,  $\lambda_{\text{max,abs}}(\text{Rh-PE}) = 560$  nm,  $\lambda_{\text{max,emi}}(\text{Rh-PE}) = 581$  nm),<sup>26</sup> pointing to interaction between the probes and the vesicles. From the spectra (and the data mentioned in the Materials and Methods section) we used eq 6 to calculate the  $R_0$  parameter for the NBD-PE/NBD-PE pair, obtaining  $R_0(25\text{ °C}) = 24.3$  Å and  $R_0(50\text{ °C}) = 21.6$  Å. For the NBD-PE/Rh-PE pair, we used the value of Wolf et al. in DOPC,  $R_0(25\text{ °C}) = 56$  Å,<sup>33</sup> which we used (together with the quantum yields, see Materials and Methods) to calculate  $R_0(50\text{ °C}) = 49.9$  Å. For the Rh-PE/Rh-PE pair, the values of Medhage et al.<sup>37</sup> in DOPC corrected for in-plane dipole distribution ( $\kappa^2 = 5/4$ ) were considered, following these authors' suggestion, 64.1 Å at 25 °C and 59.4 Å at 50 °C being obtained (the possibility of restricted rotation in the gel phase is addressed below).

**NBD-PE Energy Migration and Self-Quenching.** As mentioned in the Introduction, fluorescence polarization and self-quenching measurements were also carried out in order to obtain further information, particularly on the NBD-PE/Rh-PE system.

We studied the steady-state fluorescence intensity, average lifetime (given by  $\langle\tau\rangle = (A_1\tau_1^2 + A_2\tau_2^2)/(A_1\tau_1 + A_2\tau_2)$ ) and fluorescence anisotropy of NBD-PE:DPPC vesicles upon increasing probe concentration. Figure 2A,D show the polarization results (probe:DPPC ratios between 0.001 and 0.03). The curves in the anisotropy plots are the theoretical expectations according to Snyder and Freire<sup>39</sup> for two different values of their model's parameter  $R_0/L$ , where  $L$  is the exclusion distance for two molecules within the same plane. We also considered  $r(\text{infinite dilution}) \approx r(\text{NBD-PE:DPPC} = 0.001)$ . Assuming

$L = 8.6$  Å for NBD chromophores,<sup>40</sup> we have  $R_0/L \approx 2.83$  for the gel phase and 2.51 for the fluid phase system, so the actual theoretical anisotropy should fall between the two represented curves (valid for  $R_0/L = 2$  and 4, respectively, and triangular lattices). In any case, it is clear that for both systems (but more remarkably in the gel phase) there is more depolarization than expected by the Snyder and Freire model (i.e., with assumption of random distribution of probes). Note that only intraplanar migration is being taken into account. Transfer to NBD-PE molecules located on the opposing bilayer leaflet (interplanar migration) is being neglected. This is not a too crude approximation,<sup>41</sup> especially in the gel phase case, for which the distance between the two planes ( $\approx 44$  Å) is almost  $2R_0$ . The results suggest that the NBD-PE probes aggregate in both phases even for concentrations below  $\sim 1$  mol %. We were not able to measure reliably the anisotropy for NBD-PE:DPPC  $< 0.001$  due to weak signal, but it is very probable (especially for the gel phase) that for NBD-PE:DPPC = 0.001, the concentration used in the heterotransfer studies, aggregation already takes place to a small extent.

The decrease of  $\langle\tau\rangle$  in Figure 2C,F points to a dynamic self-quenching mechanism of NBD-PE fluorescence. The negative curvature of the fluorescence intensity plots (Figures 3B,E) is compatible with this observation, and in the Discussion section we will see whether a static mechanism (i.e. fluorophore aggregation) should also be considered to account for the steady-state variation.

**Rh-PE Energy Migration and Self-Quenching.** For Rh-PE/Rh-PE migration, interplanar transfer is no longer negligible, because of the large  $R_0$  values. For the calculation of the theoretical steady-state anisotropy in the gel phase (the most critical system regarding eventual aggregation), we adopted the two-particle model as described by Baumann and Fayer.<sup>42</sup> As Medhage et al.<sup>37</sup> observed that for this molecule the rotational lifetimes were larger than the emission lifetime, we considered only a static model (which, according to these authors, gives good agreement with a more complex model which includes the actual slow rotation of the molecule). As suggested by these authors (on the basis of linear dichroism measurements), in-plane dipole distribution is considered:

$$r(t) = (r_0 - r_\infty)G^s(t) + r_\infty \quad (8)$$

where we took  $r_0 = 0.37$  and  $r_\infty = 0.08$  from the cited reference.

The probability that an initially excited molecule is still excited at a later time  $t$ ,  $G^s(t)$  is given by

$$\ln G^s(t) = \ln G_{\text{inter}}^s(t) + \ln G_{\text{intra}}^s(t) \quad (9)$$

with

$$\ln G_{\text{intra}}^s(t) = -c(2/3)2^{-2/3}(3/2)^{1/3}\langle|\kappa|^{2/3}\rangle t^{1/3} \quad (10)$$

$$\ln G_{\text{inter}}^s(t) = -\frac{c(2/3)}{24b\pi^2\Gamma(2/3)} \int_0^1 \int_0^{2\pi} \int_0^{2\pi} \{1 - \exp[-\mu(a_1s - a_2s^{4/3} + a_3s^{5/3})]\} s^{-4/3} ds d\phi_0 d\phi_1 \quad (11)$$

where  $G_{\text{inter}}^s(t)$  and  $G_{\text{intra}}^s(t)$  are the excitation probability functions for interplanar and intraplanar transfer, respectively, and for in-plane dipole distribution, as given by Baumann and Fayer.<sup>42</sup> In eq 10,  $c(2/3)$  is the  $c$  parameter as defined in eq 2, but calculated with  $R_0$  assuming  $\kappa^2 = 2/3$ . The factor  $2^{-2/3}$  reflects the fact that we are dealing with homotransfer rather than heterotransfer (for which it would be unity), and the factor

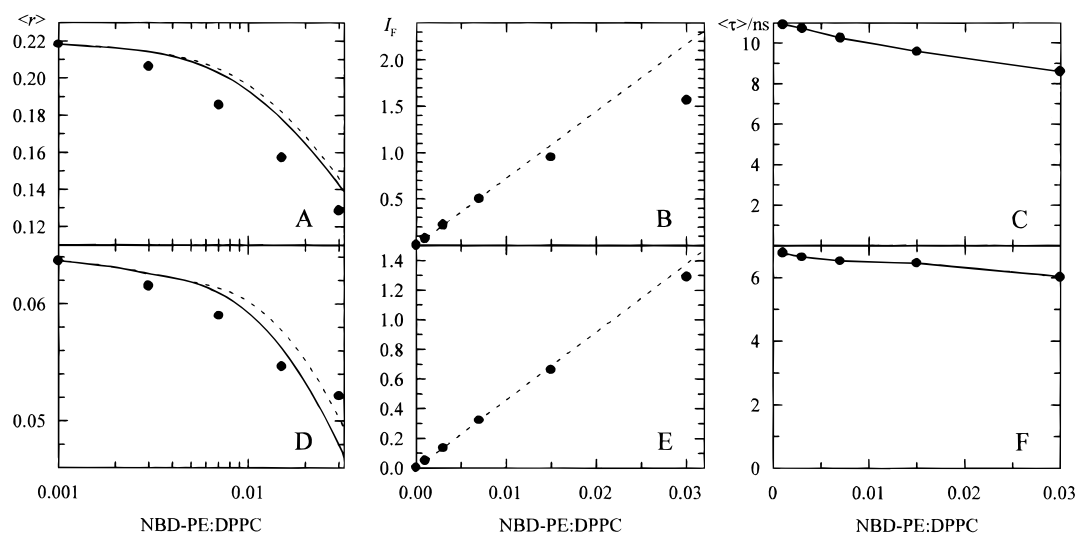


**Figure 2.** A, D: Steady-state anisotropy ( $\lambda_{\text{exc}} = 467$  nm,  $\lambda_{\text{emi}} = 537$  nm) of NBD-PE (●) in DPPC LUV at (A) 25 °C and (D) 50 °C. The theoretical curves<sup>39</sup> assuming only intraplanar migration are represented for  $R_0/L = 4$  (solid line) and  $R_0/L = 2$  (dashed line; see text). B, E: Steady-state fluorescence intensity (arbitrary units;  $\lambda_{\text{exc}} = 467$  nm,  $\lambda_{\text{emi}} = 537$  nm) of NBD-PE (●) in DPPC LUV at (B) 25 °C and (E) 50 °C. The dotted lines are linear fits excluding the two most concentrated samples. C, F: Average fluorescence lifetime of NBD-PE in DPPC LUV at (C) 25 °C and (F) 50 °C as a function of probe concentration.

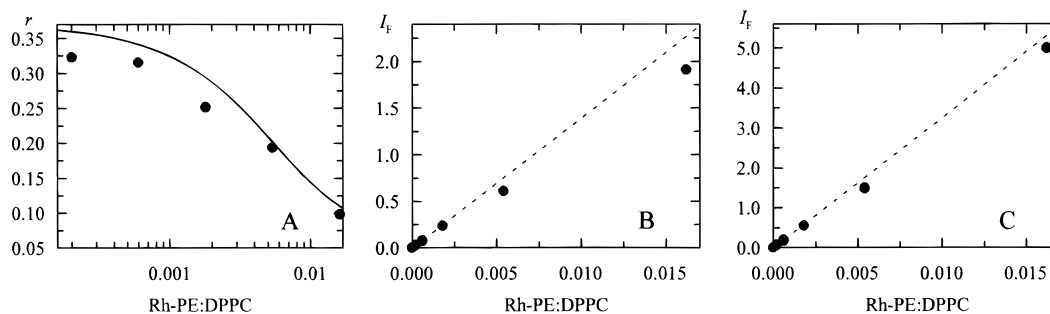


**Figure 3.** A: Steady-state anisotropy ( $\lambda_{\text{exc}} = 573$  nm,  $\lambda_{\text{emi}} = 590$  nm) of Rh-PE (●) in DPPC LUV at 25 °C. The solid line is the theoretical curve assuming a static model, in-plane dipole distribution,  $r_0 = 0.37$  and  $r_{\infty} = 0.08$ .<sup>37</sup> B, C: Steady-state fluorescence intensity (arbitrary units;  $\lambda_{\text{exc}} = 573$  nm,  $\lambda_{\text{emi}} = 590$  nm) of Rh-PE (●) in DPPC LUV at (B) 25 °C and (C) 50 °C. The dotted lines are linear fits excluding the two most concentrated samples.

$(3/2)^{1/3} \langle |K|^{2/3} \rangle$  reflects the in-plane static dipole distribution ( $\langle |K|^{2/3} \rangle = 0.9462$ ).<sup>42</sup> In eq 11,  $\mu = 3tb^3$ ,  $a_1 = 0.25(\cos(\phi_0 - \phi_1) + 3\cos(\phi_0 + \phi_1))^2$ ,  $a_2 = 1.5 \cdot (\cos(\phi_0 - \phi_1) + 3\cos(\phi_0 + \phi_1))(\cos(\phi_0 - \phi_1) + \cos(\phi_0 + \phi_1))$  and  $a_3 = 2.25(\cos(\phi_0 - \phi_1) + \cos(\phi_0 + \phi_1))^2$ . The steady-state anisotropy was calculated by integration over time of  $r(t)$ :

$$\langle r \rangle = \int_0^{\infty} r(t) i(t) dt \bigg/ \int_0^{\infty} i(t) dt \quad (12)$$

where  $i(t)$  is the fluorescence decay measured in magic angle conditions. The integrals in eq 11 and eq 12 were calculated numerically.

From comparison with the measured  $\langle r \rangle$  (Figure 3A), the experimental points lie below the theoretical curve. There is more depolarization than expected for random distribution of probes, indicating Rh-PE aggregation in the gel phase for this concentration range, which is almost the same as that in the heterotransfer experiment (see below).

Aggregation in the fluid phase is reported by Massari et al.<sup>43</sup> for very high concentration ( $>20$  mol %), and is said to be greater in the gel phase on the basis of steady-state self-quenching. Indeed, in our concentration range, the plot of fluorescence intensity versus Rh-PE concentration shows a slight negative curvature in the gel phase (Figure 3B). For Rh-PE, the lifetime value is reported to remain unchanged with increasing concentration.<sup>43</sup> Thus, the only eventual self-quench-

ing process should be of a static nature. We will address this question in the Discussion.

The authors cited above also state that the probe molecules “distribute unevenly in the bilayer surface” of gel phase vesicles on the basis of polarization measurements, but their argument ( $r(\text{gel phase}) > r(\text{fluid phase})$  for low concentrations, the reverse for high concentrations) is not valid. This observation can be alternatively explained by (1) larger infinite dilution anisotropy in the gel phase (larger rotational lifetime, making up for the increase of  $\tau$ ) and (2) larger  $R_0$  and smaller surface area for the gel phase, which results in more efficient intraplanar migration and hence more efficient depolarization for larger probe concentrations.

**Time-Resolved ET. Fluid Phase, ORB/DiIC<sub>1</sub>(7).** For DiIC<sub>1</sub>(7):outer leaflet DPPC  $\leq 0.013$  (see Table 1, Figure 4), the discrete model describes perfectly the data, acceptable fits being recovered for each decay.<sup>12</sup> In this concentration range, there is no advantage in fitting a Gaussian or sum-of-Gaussians model. The  $\chi^2$  does not improve significantly upon analysis using these latter models. The center of the Gaussian for the single Gaussian model and the two centers for the sum-of-Gaussians model match the recovered discrete concentration. The distributions are narrow, and for the single Gaussian fit, the ratio between the standard deviation and the mean value is low (average  $\sigma/\mu = 0.098$ ). Two-dimensional ET kinetics, with homogeneous distribution of acceptor, is obeyed. For the most

**TABLE 1: Results of the Global Analysis of the Decay Data for the ORB/DiIC<sub>1</sub>(7) Pair in fluid phase (50 °C) DPPC**

	D (discrete fit)	1G (single Gaussian fit)	2G (sum of Gaussians fit)
linking parameters and global $\chi^2$	$\tau_1 = 0.72$ ns $\tau_2 = 1.61$ ns $q = 2.53$ $\chi_G^2 = 1.361$	$\tau_1 = 0.80$ ns $\tau_2 = 1.65$ ns $q = 1.94$ $\chi_G^2 = 1.268$	$\tau_1 = 0.80$ ns $\tau_2 = 1.65$ ns $q = 1.96$ $\chi_G^2 = 1.255$
DiIC <sub>1</sub> (7):outer leaflet DPPC 0.0000	$\chi^2 = 1.074$	$\chi^2 = 1.111$	$\chi^2 = 1.114$
0.0022	$c = 0.244$ $\chi^2 = 1.199$	$c_1 = 0.244$ $\sigma_1 = 0.030$ $\chi^2 = 1.152$	$c_1 = 0.244$ $\sigma_1 = 0.024$ $c_2 = 0.245$ $\sigma_2 = 0.024$ $h = 1.26$ $\chi = 1.153$
0.0044	$c = 0.478$ $\chi^2 = 1.397$	$c_1 = 0.478$ $\sigma_1 = 0.035$ $\chi^2 = 1.372$	$c_1 = 0.478$ $\sigma_1 = 0.027$ $c_2 = 0.478$ $\sigma_2 = 0.027$ $h = 1.29$ $\chi^2 = 1.383$
0.0082	$c = 0.844$ $\chi^2 = 1.057$	$c_1 = 0.861$ $\sigma_1 = 0.137$ $\chi^2 = 1.063$	$c_1 = 0.723$ $\sigma_1 = 0.093$ $c_2 = 0.961$ $\sigma_2 = 0.091$ $h = 1.50$ $\chi^2 = 1.076$
0.0126	$c = 1.303$ $\chi^2 = 1.533$	$c_1 = 1.307$ $\sigma_1 = 0.049$ $\chi^2 = 1.532$	$c_1 = 1.306$ $\sigma_1 = 0.040$ $c_2 = 1.306$ $\sigma_2 = 0.040$ $h = 1.31$ $\chi^2 = 1.554$
0.0171	$c = 1.705$ $\chi^2 = 1.968$	$c_1 = 2.020$ $\sigma_1 = 0.602$ $\chi^2 = 1.476$	$c_1 = 1.944$ $\sigma_1 = 0.034$ $c_2 = 0.014$ $\sigma_2 = 0.032$ $h = 0.039$ $\chi^2 = 1.353$

concentrated sample (DiIC<sub>1</sub>(7): outer leaflet DPPC = 0.017), some degree of heterogeneity becomes apparent. In fact, for the discrete concentration fit,  $\chi^2$  increases significantly. The negative error in the recovery of  $c$  might indicate an increase of width of the concentration distribution (see preceding article). This is indeed the case, as shows the fit to a Gaussian distribution ( $\sigma/\mu = 0.30$ ). In any case, the distribution remains unimodal, as can be seen from the sum-of-Gaussians fit, which improves only slightly the  $\chi^2$  value and leads to almost no change in the curves (therefore, for the sake of clarity, these are not shown in Figure 4). Consideration of the model of isolated donors (fixing  $c_2 = 0$  and optimizing  $c_1$ , see eq 3) does not improve the goodness of the fit either (results not shown).

**Fluid Phase, NBD-PE/Rh-PE.** For this pair (see Table 2, Figure 5), some heterogeneity is observed at lower concentrations. For Rh-PE:DPPC = 0.0073, there is already a negative bias in the recovery of  $c$  and the recovered Gaussian standard deviations are wider (average  $\sigma/\mu = 0.21$ ). All  $\chi^2$  values improve significantly from the discrete concentration model to the single Gaussian model. Again, a sum-of-Gaussians model (optimizing  $c_1$  and  $c_2$ ) does not improve the goodness of fit considerably or change significantly the recovered distributions (therefore, and for the sake of clarity, these are not shown in Figure 5), and consideration of isolated donors (fixing  $c_2 = 0$ ) leads to no improvement of  $\chi^2$  (results not shown).

We would like to make a brief comment about the  $R_0$  and  $b$  values for this system. Unlike for the planar system, where the  $R_0$  value is not an input of the program, the bilayer geometry algorithms need an input value of  $b = (R_0/w)\tau^{-1/3}$ , which, as mentioned in the preceding article, is not optimized throughout the analysis. However, just as in the planar case,<sup>12</sup> one can

calculate an output  $R_0$  value from the slope of the plot of the recovered  $c$  values against acceptor density. If our assumed input  $R_0$  value were not correct, say too small, then the program tends to make up for this systematic error by recovering larger  $c$  values. From these values, the output  $R_0$  value will be too large, and conversely for too large  $R_0$  input values. A satisfactory input  $R_0$  will result in an almost identical output value, differing less than a tolerance limit of, say, 1 Å. We applied this procedure to the single-Gaussian fitting program, using the centers of distributions' values to obtain  $R_0(50\text{ °C}) \approx 55$  Å. This value was used to determine  $R_0(25\text{ °C}) \approx 62$  Å,  $b(50\text{ °C}) = 1.18$  ns<sup>-1/3</sup> and  $b(25\text{ °C}) = 0.773$  ns<sup>-1/3</sup>. The  $b$  values were in turn used in the analysis of all NBD-PE/Rh-PE data (see Discussion).

**Gel Phase, ORB/DiIC<sub>1</sub>(7).** For the ORB/DiIC<sub>1</sub>(7) pair, we recently reported that no satisfactory fit could be obtained for a planar, discrete concentration model.<sup>12</sup> The single Gaussian model also fails (see Table 3), very broad distributions being recovered, centered either at negative values (for the lower acceptor densities) or at very large, unrealistic values (for the higher acceptor densities). For some samples,  $\chi^2$  is acceptable, but the width of the distributions and the unrealistic center values indicate that the actual distributions might be quite different. This is indeed verified by looking at the recovered sum-of-Gaussians distributions (Figure 6). For reasons which are not entirely clear, when both  $c_1$  and  $c_2$  are allowed to float, non significant values are recovered for  $c_1$  ( $\sim 20$ ) and  $\sigma_1$  ( $\sim 80$ ) for DiIC<sub>1</sub>(7):outer leaflet DPPC = 0.0044. However, these values do not actually imply an unmeaningful distribution, because of the small amplitude (18%) of this Gaussian. In any case, and because for all samples a peak near  $c = 0$  is recovered (see Table 4), we repeated the two Gaussian fit, this time having fixed  $c_2 = 0$ . Apart from the change in the  $c_1$  and  $\sigma_1$  parameters of the DiIC<sub>1</sub>(7): outer leaflet DPPC = 0.0044 curve (not so much the actual curve), the results and  $\chi^2$  values are essentially unchanged ( $\chi_G^2 = 1.147$  before fixing  $c_1 = 0$ , and  $\chi_G^2 = 1.148$  after this procedure, see Table 3). For DiIC<sub>1</sub>(7):outer leaflet DPPC  $\leq 0.0082$ , the distribution maximum is located at  $c = 0$ , a secondary peak at larger concentrations becoming more important upon increasing concentration. For DiIC<sub>1</sub>(7):outer leaflet DPPC  $\geq 0.0126$ , the large concentration peak becomes the absolute maximum, and the peak at  $c = 0$  virtually vanishes.

**Gel Phase, NBD-PE/Rh-PE.** Unlike the fluid phase, the gel phase results of the NBD-PE/Rh-PE pair are very different from those of the ORB/DiIC<sub>1</sub>(7) pair for the same phase (see Table 4, Figure 7). This is not noticeable from the discrete (for which the  $c$  vs bulk concentration variation shows strong negative curvature) and single Gaussian fits (for which most recovered distributions are tails of Gaussians centered at some negative  $c$  value), but is immediately apparent from the sum-of-two Gaussians ones (the only global fits which have acceptable  $\chi^2$ ). For every sample, there are two perfectly separated peaks. One peak is centered at a large, approximately constant  $c_2$  value, while the other peak is centered at linearly increasing (upon increasing acceptor density)  $c_1$  values, comparable to those recovered from the discrete fit. Fixing  $c_1 = 0$  results in divergence of the program.

**Steady-State Quenching of NBD-PE by Rh-PE.** Time-resolved ET measurements alone are unable to detect very fast quenching resulting from association of donor and acceptor molecules. To check if these static quenching processes are operative in our systems, we should perform both time-resolved and steady-state ET measurements. For the ORB/DiIC<sub>1</sub>(7) pair, static quenching was ruled out elsewhere and no evidence for

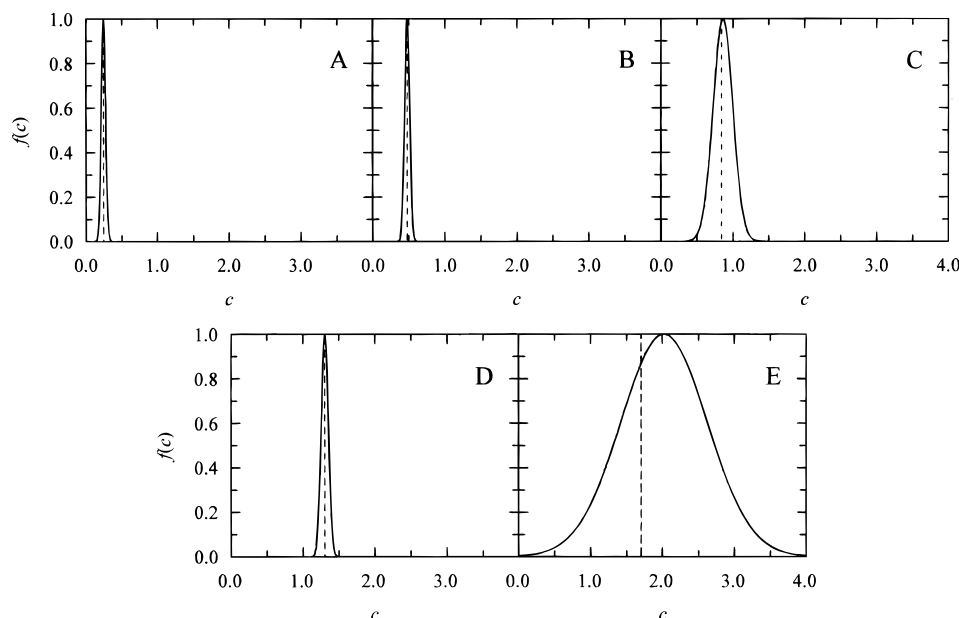


**Figure 4.** Acceptor concentration distributions recovered for the ORB decay data in fluid phase DPPC LUV (50 °C) in the presence of different amounts of DiIC<sub>1</sub>(7) (ratios DiIC<sub>1</sub>(7) to outer leaflet DPPC: A, 0.0022; B, 0.0044; C, 0.0082; D, 0.0126; E, 0.0171). The vertical dotted lines represent the  $c$  values recovered for the discrete fit, and the solid line are the Gaussian curves recovered by program 1G.

**TABLE 2: Results of the Global Analysis of the Decay Data for the NBD-PE/Rh-PE Pair in Fluid Phase (50 °C) DPPC**

	D (discrete fit)	1G (single Gaussian fit)	2G (sum of Gaussians fit)
linking parameters and global $\chi^2$	$\tau_1 = 0.68$ ns $\tau_2 = 6.62$ ns $q = 2.33$ $\chi_G^2 = 2.703$	$\tau_1 = 0.81$ ns $\tau_2 = 6.58$ ns $q = 2.97$ $\chi_G^2 = 1.226$	$\tau_1 = 0.79$ ns $\tau_2 = 6.58$ ns $q = 2.94$ $\chi_G^2 = 1.181$
Rh-PE:DPPC			
0.0000	$\chi^2 = 1.391$	$\chi^2 = 1.199$	$\chi^2 = 1.201$
0.0020	$c = 0.170$ $\chi^2 = 1.397$	$c_1 = 0.174$ $\sigma_1 = 0.032$ $\chi^2 = 1.167$	$c_1 = 0.172$ $\sigma_1 = 0.016$ $c_2 = 0.172$ $\sigma_2 = 0.016$ $h = 0.993$ $\chi^2 = 1.163$
0.0040	$c = 0.382$ $\chi^2 = 1.434$	$c_1 = 0.387$ $\sigma_1 = 0.023$ $\chi^2 = 1.141$	$c_1 = 0.388$ $\sigma_1 = 0.012$ $c_2 = 0.384$ $\sigma_2 = 0.013$ $h = 1.75$ $\chi^2 = 1.142$
0.0073	$c = 0.633$ $\chi^2 = 1.310$	$c_1 = 0.724$ $\sigma_1 = 0.192$ $\chi^2 = 1.159$	$c_1 = 0.623$ $\sigma_1 = 0.090$ $c_2 = 0.766$ $\sigma_2 = 0.222$ $h = 1.10$ $\chi^2 = 1.075$
0.0121	$c = 0.960$ $\chi^2 = 8.019$	$c_1 = 1.450$ $\sigma_1 = 0.499$ $\chi^2 = 1.487$	$c_1 = 1.178$ $\sigma_1 = 0.022$ $c_2 = 8.930$ $\sigma_2 = 4.43$ $h = 0.029$ $\chi^2 = 1.263$

donor-acceptor complexes was found.<sup>12</sup> Regarding the NBD-PE/Rh-PE pair, in Figure 8 we compare the relative NBD-PE fluorescence intensities in the presence of varying amounts of Rh-PE as obtained in a steady-state experiment with those obtained by integration of the experimental decays. While for the fluid phase system (Figure 8A) a small degree of static quenching becomes apparent only for Rh-PE:DPPC = 1:80, for the gel phase all samples show appreciably more quenching

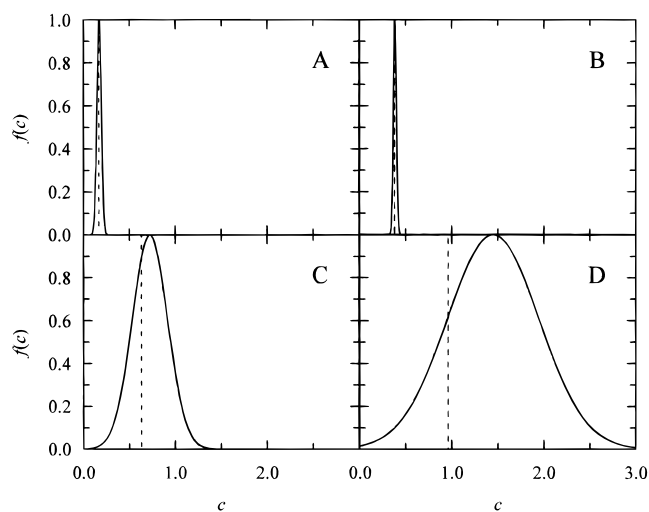


**Figure 5.** Acceptor concentration distributions recovered for the NBD-PE decay data in fluid phase DPPC LUV (50 °C) in the presence of different amounts of Rh-PE (ratios Rh-PE to DPPC: A, 0.0020; B, 0.0040; C, 0.0073; D, 0.0121). The lines have the same meaning as in Figure 4.

in the steady-state experiment than in the time-resolved measurements. The fluid phase result is at variance with that reported by Lantzsch et al.,<sup>19</sup> who observed greater steady-state efficiency than that calculated from decay integration. However, as referred by the cited authors, their result is most probably due to reabsorption of donor emission by Rh-PE, and this effect was corrected in our plot.

## 5. Discussion

**NBD-PE Energy Migration and Self-Quenching.** As mentioned in the Results section, the analysis of energy migration among NBD-PE molecules in both phases points to a nonrandom distribution of probes, and we now address the question of NBD-PE fluorescence self-quenching. The self-quenching of NBD-labeled probes, namely NBD-PE derivatives, is well documented and has been used for various purposes, including domain detection in vesicles.<sup>44</sup> Figure 2C,F



**TABLE 3: Results of the Global Analysis of the Decay Data for the ORB/DiIC<sub>1</sub>(7) Pair in Gel Phase (25 °C) DPPC**

	D (discrete fit)	1G (single Gaussian fit)	2G ( $c_2 = 0$ , fixed)
linking	$\tau_1 = 0.44$ ns	$\tau_1 = 0.75$ ns	$\tau_1 = 0.74$ ns
parameters and global $\chi^2$	$\tau_2 = 2.95$ ns $q = 2.20$ $\chi_G^2 = 8.382$	$\tau_2 = 3.00$ ns $q = 2.59$ $\chi_G^2 = 1.755$	$\tau_2 = 2.94$ ns $q = 2.95$ $\chi_G^2 = 1.148$
DiIC <sub>1</sub> (7): outer leaflet DPPC			
0.0000	$\chi^2 = 5.500$	$\chi^2 = 1.383$	$\chi^2 = 1.165$
0.0022	$c = 0.291$ $\chi^2 = 3.153$	$c_1 = -0.0730$ $\sigma_1 = 0.502$ $\chi^2 = 1.194$	$c_1 = -0.349$ $\sigma_1 = 1.194$ $\sigma_2 = 0.130$ $h = 3.680$ $\chi^2 = 1.117$
0.0044	$c = 0.495$ $\chi^2 = 1.684$	$c_1 = -1.381$ $\sigma_1 = 1.610$ $\chi^2 = 1.155$	$c_1 = 0.658$ $\sigma_1 = 1.139$ $\sigma_2 = 0.136$ $h = 2.292$ $\chi^2 = 1.082$
0.0082	$c = 1.412$ $\chi^2 = 3.023$	$c_1 = 2.362$ $\sigma_1 = 1.061$ $\chi^2 = 1.039$	$c_1 = 2.064$ $\sigma_1 = 0.357$ $\sigma_2 = 0.021$ $h = 1.376$ $\chi^2 = 0.991$
0.0126	$c = 1.949$ $\chi^2 = 12.44$	$c_1 = 5.969$ $\sigma_1 = 2.256$ $\chi^2 = 2.101$	$c_1 = 2.892$ $\sigma_1 = 0.127$ $\sigma_2 = 0.011$ $h = 0.515$ $\chi^2 = 1.186$
0.0171	$c = 2.094$ $\chi^2 = 25.03$	$c_1 = 6.999$ $\sigma_1 = 2.743$ $\chi^2 = 3.777$	$c_1 = 3.483$ $\sigma_1 = 0.087$ $\sigma_2 = 0.0042$ $h = 0.388$ $\chi^2 = 1.427$

indicate dynamic self-quenching of NBD-PE fluorescence in DPPC LUV. These data can be rationalized according to a simplified Stern-Volmer formalism, with consideration of average lifetimes:

$$\langle\tau_0\rangle/\langle\tau\rangle = 1 + k_Q\langle\tau_0\rangle[F] \quad (13)$$

where  $\langle\tau_0\rangle$  is the average lifetime at infinite dilution,  $k_Q$  is the collisional quenching rate constant, and  $[F]$  is the fluorophore concentration. The equation for steady-state self-quenching, allowing for both dynamic and static (model of active sphere of quenching) contributions, is given below.<sup>45</sup>

$$I_F = \frac{k[F]}{1/\tau_0 + k_Q[F]} \exp(-VN_A[F]) \quad (14)$$

In this equation, the first term reflects the dynamic contribution (expressed in eq 13), and the second represents an active sphere static component ( $k \propto I_0\epsilon k_F l$  in dilute solution, where  $I_0$  is the incident light intensity,  $\epsilon$  is the fluorophore molar absorptivity,  $k_F$  is its radiative decay rate constant, and  $l$  is the optical path;  $V$  is the active sphere volume and  $N_A$  is Avogadro's number).

For the gel phase, fitting of eq 13 to the lifetime data (Figure 2C) gives  $k_Q = 6.6 \times 10^7 \text{ M}^{-1} \text{ s}^{-1}$ . Introduction of this value in eq 16 and subsequent fitting of the steady-state data (Figure 3B) results in a value of  $R_s = (V/(4/3\pi))^{1/3} = 12 \text{ \AA}$  for active sphere radius. This value is slightly higher than the estimated collisional radius for two NBD chromophores (8.6  $\text{\AA}$ ).<sup>40</sup> As the contribution of transient effects in increasing  $V$  is small, this observation indicates that the association is more efficient than the one accounted for by the active sphere formulation. A complexation treatment could be invoked; however, for the aim of the present analysis, that additional treatment is not necessary.

The important conclusion is that NBD-PE aggregates in the gel phase. On the other hand, from  $k_Q$  and the Smoluchowski equation for collision of molecules of a single species (and taking into account transient effects),<sup>40</sup>

$$k_Q = 4\pi N_A(2R)\gamma(2D)[1 + 2R/(\tau_0(2D))^{1/2}] \quad (15)$$

we can in principle estimate the diffusion coefficient  $D$  ( $R$  is the collision radius, taken as 4.3  $\text{\AA}$ ,<sup>40</sup> and  $\gamma$  is the quenching efficiency of the reaction, taken as unity). A value of  $D = 6.0 \times 10^{-9} \text{ cm}^2 \text{ s}^{-1}$  is obtained (it will be discussed in the gel phase ET Discussion subsection).

For the fluid phase, this rationalization could not be worked out, because the lifetime variation upon increasing concentration is small (Figure 2F), and led to imprecise recovery of  $k_Q$  in eq 13.

In summary, from the variation of  $r$ ,  $I_F$ , and  $\langle\tau\rangle$  in the 0.1–3 mol % concentration range, NBD-PE aggregation in the gel phase can be safely invoked. For the fluid phase, only the  $r$  data point to a nonrandom distribution, and no clear evidence for aggregation is obtained.

**Rh-PE Energy Migration and Self-Quenching.** As mentioned in the results section, the energy migration results indicate nonrandom distribution of Rh-PE in the gel phase. On the other hand, from the lifetime invariance upon increasing concentration, only static quenching might be operative. This can be verified by analyzing the steady-state intensity with eq 14, fixing  $k_Q = 0$ . A slight negative  $R$  value is recovered for the gel phase, probably due to limited precision of the data. This does not necessarily mean that aggregation is absent. From inspection of Figure 3B, it can be seen that the two highest concentration points lie below the straight line derived from the other (dilute concentration) points, even though a negative curvature was not obtained upon consideration of all samples. For the fluid phase, the plot in Figure 3C is almost linear, and self-quenching is negligible.

In conclusion, Rh-PE aggregation cannot be ruled out, especially for the gel phase, where deviations from linearity in the  $I_F$  plot are larger, and the variation of  $\langle r \rangle$  with probe concentration points to nonrandom distribution.

**Fluid Phase ET.** From the time-resolved ET results section, it is clear that the fluid phase decays can be well described by classical, discrete-concentration kinetics for moderate acceptor concentrations. For the NBD-PE/Rh-PE pair, distributions are generally wider than for the ORB/DiIC<sub>1</sub>(7) pair, revealing a larger degree of heterogeneity. Additionally, the threshold concentration for which a discrete model returns negatively biased  $c$  values (indicating nonrandomness of probe distribution<sup>46,47</sup>) and it becomes necessary to consider a distribution model in order to recover acceptable  $\chi^2$  values is lower for the former pair. Although the distribution function is that of acceptor concentration, the ET decay curve involves all donor molecules. In this way, a heterogeneous curve may arise from both acceptor and (in the case of a finite system or coexisting acceptor nonhomogeneity) donor nonrandom distributions. The net effect is a widening of the acceptor concentration distribution. The lower ideality of the distributions recovered for the NBD-PE/Rh-PE pair relative to those recovered for the ORB/DiIC<sub>1</sub>(7) pair could therefore be caused by less random donor distributions, acceptor distributions, or both.

On one hand, ORB is thought to distribute evenly on the bilayer for concentrations  $< 0.4$  mol % on the basis of its depolarization curve.<sup>12</sup> For NBD-PE, the same plot reveals more depolarization than expected from the Snyder and Freire<sup>39</sup> curve, which means that the nearest neighbor of a NBD-PE



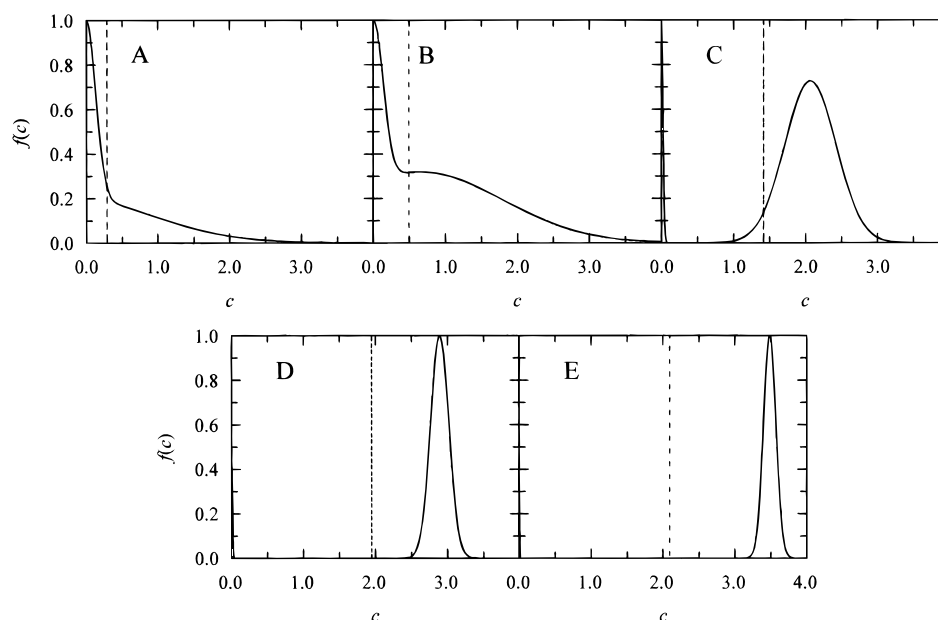


**Figure 6.** Acceptor concentration distributions recovered for the ORB decay data in gel phase DPPC LUV (25 °C) in the presence of different amounts of DiIC<sub>1</sub>(7) (the letters and lines have the same meaning as in Figure 4, except the solid lines, which are the functions recovered by program 2G with fixed  $c_2 = 0$ ).

**TABLE 4: Results of the Global Analysis of the Decay Data for the NBD-PE/Rh-PE Pair in Gel Phase (25 °C) DPPC**

	D (discrete fit)	1G (single Gaussian fit)	2G (sum of Gaussian fit)
linking parameters and global $\chi^2$	$\tau_1 = 2.06$ ns $\tau_2 = 11.72$ ns $q = 1.81$ $\chi_G^2 = 3.001$	$\tau_1 = 3.27$ ns $\tau_2 = 11.73$ ns $q = 2.22$ $\chi_G^2 = 2.007$	$\tau_1 = 5.33$ ns $\tau_2 = 12.86$ ns $q = 1.24$ $\chi_G^2 = 1.282$
Rh-PE:DPPC			
0.0000	$\chi^2 = 4.773$	$\chi^2 = 2.178$	$\chi^2 = 2.063$
0.0020	$c = 0.128$ $\chi^2 = 2.210$	$c_1 = -4.023$ $\sigma_1 = 0.933$ $\chi^2 = 2.239$	$c_1 = 0.0879$ $\sigma_1 = 0.0149$ $c_2 = 1.810$ $\sigma_2 = 0.0080$ $hT = 2.39$ $\chi^2 = 1.215$
0.0040	$c = 0.220$ $\chi^2 = 2.360$	$c_1 = -12.3$ $\sigma_1 = 2.67$ $\chi^2 = 1.677$	$c_1 = 0.176$ $\sigma_1 = 0.0828$ $c_2 = 1.915$ $\sigma_2 = 0.0124$ $h = 12.0$ $\chi^2 = 1.026$
0.0073	$c = 0.306$ $\chi^2 = 2.359$	$c_1 = -0.130$ $\sigma_1 = 1.064$ $\chi^2 = 1.656$	$c_1 = 0.239$ $\sigma_1 = 0.0306$ $c_2 = 2.138$ $\sigma_2 = 0.0176$ $h = 4.45$ $\chi^2 = 1.029$
0.0121	$c = 0.414$ $\chi^2 = 3.339$	$c_1 = 0.648$ $\sigma_1 = 0.391$ $\chi^2 = 2.320$	$c_1 = 0.411$ $\sigma_1 = 0.139$ $c_2 = 2.553$ $\sigma_2 = 0.0243$ $h = 14.0$ $\chi^2 = 1.094$

molecule is, on the average, closer than expected for a random distribution. For the ORB/DiIC<sub>1</sub>(7) pair, we were able to use a lower donor concentration by an order of magnitude relative to that of NBD-PE (ORB:DPPC = 0.0001), due to the simultaneously higher fluorescence quantum yield and absorption at convenient excitation wavelengths of the rhodamine chromophore. A reduction of the NBD-PE concentration would be desirable but is prevented in our case by the low fluorescence signal. However, in any case, the eventual energy migration for NBD-PE:DPPC = 0.001 would still not be enough to hamper the presented heterotransfer data.

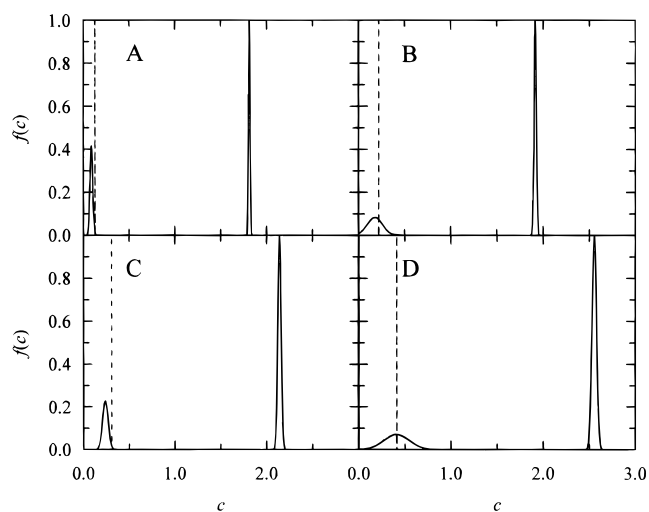


**Figure 7.** Acceptor concentration distributions recovered for the NBD-PE decay data in gel phase DPPC LUV (25 °C) in the presence of different amounts of Rh-PE (the letters and lines have the same meaning as in Figure 5, except the solid lines, which are the functions recovered by program 2G).

On the other hand, it could be argued that, due to its acyl chains, Rh-PE penetrates more deeply in the membrane than DiIC<sub>1</sub>(7) (which lacks an aliphatic tail), and thus could cause more membrane perturbation. This could in turn affect the distribution function. In fact, for micelles, it was reported that a perturbed site resulting from probe incorporation becomes a region of enhanced probability of location of other probe molecules.<sup>31</sup> This type of effect, which could take place for Rh-PE:DPPC  $\geq 0.015$  (Figure 4E), would add to the donor heterogeneity effect.

In conclusion, fluid phase heterogeneity is not important for moderate concentrations for both pairs. This was already verified by Lantzsch et al.<sup>19</sup> and Loura et al.,<sup>12</sup> who were able to analyze their ET data for the NBD-PE/Rh-PE and ORB/DiIC<sub>1</sub>(7) pairs, respectively, with a discrete model (which, as shown in the preceding article, would fail if the distributions were wide). No evidence for static quenching (which could indicate a donor-

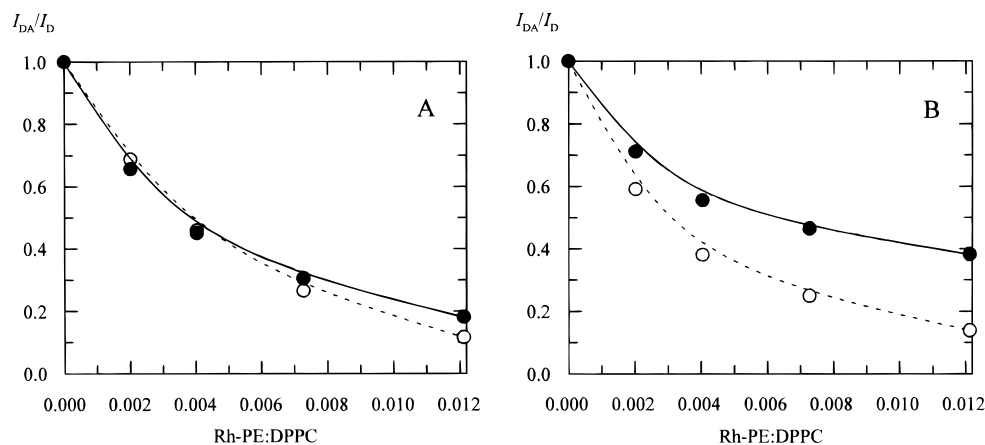


**Figure 8.** Steady-state (○) and integrated time-resolved (●) ET quenching ratios  $I_{DA}/I_D$  for the NBD-PE/Rh-PE pair in DPPC LUV, at (A) 50 °C and (B) 25 °C. The curves are mere guides to the eye.

acceptor association at a molecular distance level) is observed for moderate concentrations, even for NBD-PE/Rh-PE. Together, our results confirm that fluid phase model membranes behave as almost ideal solvents for these probes.

**Gel Phase ET.** The intriguing impossibility to fit the ORB/DiIC<sub>1</sub>(7) gel phase ET decays to the classical, discrete-concentration model, at variance with the fluid phase, was the fact that led us to consider more general models. One of them, the isolated donors model (see eq 3 in the preceding article), which could fit to the data adequately,<sup>12</sup> was a precursor of the distribution formalism applied in this work. Another step was the single-Gaussian model, which could recover symmetric wide distributions,<sup>11</sup> but also failed to fit to the gel phase data for both ORB/DiIC<sub>1</sub>(7) and NBD-PE/Rh-PE pairs, tails of Gaussians being recovered for most cases. This alerted us to the fact that the gel phase distributions should be asymmetric and/or bimodal and led us to consider the sum-of-two-Gaussians extension. Up to this stage of analysis, the results for the two systems looked similar. The sum-of-two-Gaussians model allows, for the first time, to clearly draw differences between them.

On one hand, the ORB/DiIC<sub>1</sub>(7) pair is characterized by having “isolated donors” for the samples with low overall acceptor concentration. This type of distributions resembles that of the dye aggregation in polymer films presented by Liu et al.<sup>20</sup> The distribution maximum for our samples is located at  $c = 0$ . Depolarization experiments indicated that ORB does not aggregate in the gel phase for the studied donor concentration.<sup>12</sup> The isolation of donors thus seems to be caused not by actual segregation of donors, but by segregation of acceptors instead. We proposed that this segregation would occur in defects in the gel lattice. In agreement, we showed in Monte Carlo simulation 3 of the preceding paper that a small total concentration of acceptors (similar to that of the most diluted sample in this study), together with segregation of acceptors (but not donors) to the lines of a square grid (size of each square  $\sim 20 R_0$  or 1000 Å; see Figure 1C of the preceding paper), led to a bimodal acceptor concentration distribution, with isolated donors (see Figure 2C of the preceding paper). We also tried different square sizes in those simulations; for sizes smaller than  $\sim 10 R_0$  or 500 Å, the “isolated donors” peak is located at a small but finite abscissa (result not shown), unlike the experimental results. We can therefore set this value as a lower limit for the actual size.

With increasing acceptor concentration, less donors are isolated and the distribution would gradually become unimodal. In the Monte Carlo simulations of the preceding paper, we verified that, for the chosen grid size, crowding of the lines

with a very large amount of acceptors did not lead to a unimodal distribution, but rather to a bimodal one, in which the abscissa of the first peak is no longer zero, but is still far from that of the other peak (result not shown). As mentioned above, a smaller grid size, which would possibly lead to unimodal distributions for large total acceptor concentrations, did not lead to isolated donors for low acceptor concentrations (and was thus deemed unacceptable). To explain these observations, we propose that the appearance of a unimodal distribution at large acceptor concentrations is due to a “defect saturation” effect. If above a given concentration the linear defects become saturated with acceptors, and further addition of acceptors would only lead to their placement inside the gel lattice, the distribution becomes unimodal for large concentrations. This agrees with Monte Carlo simulation 4 of the preceding article (see Figures 1D and 2D).

The fact that no static quenching is observed, i.e., no donor-acceptor complexes are formed, corroborates the hypothesis that donors do not segregate to defects (where they could possibly be located within molecular distances of an acceptor molecule). In conclusion, the results are compatible with partial segregation of acceptor into a pseudo (defect) phase and random dispersion of donors in the (bulk) gel lattice.

On the other hand, for the NBD-PE/Rh-PE pair, two well separated peaks are recovered for all samples, a first one located at small  $c$  values that increase linearly with overall acceptor concentration, and a second one located at high and almost unchanging (slightly increasing)  $c$  values. These two peaks represent donor molecules in very different environments, characterized by two distinct acceptor concentrations. One possibility is that the second peak corresponds to donors segregated in lattice defects, surrounded by a high local concentration of acceptors (which would also segregate), and the first peak corresponds to donors located in the bulk gel lattice, surrounded by a smaller concentration of acceptors. Monte Carlo simulation 5 of the preceding article was run in such premises, and the distributions recovered by analysis (using models 2G, 1G, and D alike) of the simulated decay are quite similar to those recovered from experiment (bimodal Gaussians for 2G analysis, Gaussians centered at negative values for 1G analysis, values slightly above the smaller peak for D analysis; compare part 5 of Figure 2 of the preceding article with Figure 7 in this paper).

The relative amounts of both probes in both “phases”, as well as the ratio of areas of each “phase”, could in principle be calculated. If we assume a simple partition model of donors and acceptors into two pseudo-phases, the defects/lattice coefficient partition of acceptors would simply be

$$K_{pA} = c_2/c_1 \quad (16)$$

where  $c_2$  and  $c_1$  are given in Table 4, and are proportional to the mean concentration of acceptors in the defects and outside them, respectively. From the acceptor mass balance, the fraction of area associated to the defects would be given by

$$a = (c_b - c_1)/(c_2 - c_1) \quad (17)$$

where  $c_b$  is proportional to the (mean) bulk concentration of acceptors and can be calculated using again eq 2 with the expected value for  $n_{2A}$  for a random distribution. Finally, being the ratio  $I_2/I_1$  of the integrated  $c_2$  peak to the integrated  $c_1$  peak is equal to the ratio of donors which experience each environment, it is easy to show from the donor mass balance that the defects/lattice partition coefficient of donors should be given by

$$K_{pD} = ((1 - a)/a)(I_2/I_1) \quad (18)$$

From our results, we calculated  $a = 0.3 \pm 0.2$ ,  $K_{pA} = 12 \pm 6$ , and  $K_{pD} = 11 \pm 8$  (the errors are the values of standard deviation for the set of four samples). These results should be taken as very rough estimates, because, as shown in the preceding article, the analysis of experimental (noisy) samples, may not always lead to accurate results. Furthermore, eqs 16–18 are ill-conditioned with respect to the input values of  $c_1$ ,  $c_2$ ,  $I_1$ , and  $I_2$ , meaning that small errors in these parameters may lead to appreciably larger errors in  $a$ ,  $K_{pA}$ , and  $K_{pD}$ , which is also reflected in the large standard deviations associated with the parameters. The large defect-associated area may in fact be an overestimate. Assuming that the main defects on the gel phase lattice are linear,<sup>2</sup> they should actually have a very small area. However, the used formalism (eqs 1–5) accounts for ET in all directions in the plane. As a result, the defects are sensed not as lines with essentially zero area, but necessarily as two-dimensional regions (centered around the fraction of donors that senses large mean local acceptor concentration), which should contain not only the actual defect lines, but also a not negligible regular bulk region. In the preceding article, we verified that it was not possible to calculate  $a$  accurately from ET analysis in the case of segregation into lines, even when one can still get good estimates of  $K_{pA}$  and  $K_{pD}$ . The large standard deviations of  $K_{pA}$ ,  $a$ , and  $K_{pD}$  are also due to the fact that  $c_1$  increases linearly with acceptor concentration, while  $c_2$  increases much less in relative terms (this results in an increase of the calculated  $a$  and a decrease of  $K_{pA}$  and  $K_{pD}$  for larger acceptor concentration). In turn, this latter phenomenon is a verification of saturation of the available defect sites for increasing acceptor concentration, similar to the effect invoked above for the ORB–DiIC<sub>1</sub>(7) pair.

One can, in any case, conclude that the amounts of both donors and acceptors are not negligible in both environments. The fact that both donor and acceptor show self-quenching also indicates that both probes undergo partial self-aggregation, and the static-quenching indicates that donor–acceptor complexes are formed. This is consistent with segregation of both probes into a restricted environment, possibly lattice defects. In conclusion, the results are compatible with partial segregation of both donor and acceptor into a pseudo (defect) phase.

The segregation of NBD–PE and DiI-type probes in defects is not a novel idea and has been proposed as an explanation for the recovery of two very distinct diffusion coefficients for these probes in FRAP experiments.<sup>48–50</sup> A very small coefficient is ascribed to probes located in the “bulk” and a larger coefficient,

comparable to the fluid phase values, is interpreted as caused by molecules diffusing along gel lattice defects. It is now opportune to compare the value  $D = 6.0 \times 10^{-9} \text{ cm}^2 \text{ s}^{-1}$  we obtained for  $D(\text{NBD–PE}, 25^\circ \text{C})$  with the FRAP studies. The order of magnitude of our value is the same of the large diffusion component in those works ( $10^{-8}$ – $10^{-10} \text{ cm}^2 \text{ s}^{-1}$ ), which could indicate that the dynamic self-quenching of NBD–PE fluorescence occurs mainly due to a fraction of probes diffusing along defects. Note that our value is biased by the fact that we are introducing the overall concentration of NBD–PE in eq 13, which would not be correct if the diffusing probes responsible for the dynamic self-quenching were confined to structural defects. The error in concentration brought by this procedure could possibly be of up to about an order of magnitude, and  $D$  would be overestimated by the same factor. In any case,  $D$  would still fall close to the FRAP values for the fast diffusing component.

It is reasonable to conclude that while NBD–PE/Rh–PE can be used cautiously as an almost ideal ET pair in model fluid membranes for low donor concentration ( $\sim 0.1\%$  or less) and acceptor concentrations up to approximately 1%, they should not be used, at least for quantitative purposes, in gel phase membranes. The question is, given the nonsmooth nature of the gel phase, whether a good gel phase membranes ET pair exists or not. To our knowledge, all gel phase ET studies (which are rare) have shown deviations from classical ET kinetics. In any case, a systematic effort in search of probes which might disperse randomly in the gel phase and have suitable spectroscopic properties has not been conducted yet. One possibility, which we are studying, is the use of long-tailed DiI carbocyanine dyes, which are reported to prefer the gel phase rather than the fluid phase<sup>51,52</sup> and to diffuse unimodally in FRAP experiments at temperatures  $\sim 20^\circ \text{C}$  below the main transition temperature for dimyristoylphosphatidylcholine.<sup>48</sup> These probes' absorption and emission wavelengths are modulated by the length of the spacing chain, which increases the possibilities of the use of at least one such dye as a half of a gel phase ET pair. ORB might be a good substitute for Rh–PE, and replacement of NBD–PE as a possible donor in the 500–550 emission range may be accomplished (subject to testing) with fluorescein-based probes or other suitable chromophores.

Finally, we would like to comment on the  $R_0$  value used (and recovered) in the analysis of NBD–PE/Rh–PE decay data. The procedure for obtaining a consistent value was described in the Results section, together with the values, which are surprisingly high ( $R_0(50^\circ \text{C}) \approx 55 \text{ \AA}$ ,  $R_0(25^\circ \text{C}) \approx 62 \text{ \AA}$ ). Wolf et al.<sup>33</sup> reported the spectroscopic value  $R_0(\text{room temperature}) = 56 \text{ \AA}$  for this pair in DOPC (fluid phase). However, they went on to recover  $R_0 = 66 \text{ \AA}$  after analysis of steady-state data. Were their measurements performed in a gel phase membrane, one could invoke static quenching for this discrepancy. As their vesicles were in the fluid phase, it must be concluded that the spectroscopic value of  $R_0$  is too low. In agreement with these authors, we propose that the major source of uncertainty is the orientation factor ( $\kappa^2$ ) value. Medhage et al.<sup>37</sup> showed that in-plane dipole distribution was expected for Rh–PE/Rh–PE migration on the basis of linear dichroism measurements, and this distribution explained their time-resolved anisotropy results. However, to our knowledge, no such information is available for NBD–PE. If NBD–PE's dipole distribution is approximately in-plane, we should consider  $\kappa^2 = 5/4$  instead of the isotropic  $2/3$  value used by Wolf et al. in their spectroscopic  $R_0$  calculation. This would lead to  $R_0(50^\circ \text{C}) = 55.4 \text{ \AA}$  and  $R_0(25^\circ \text{C}) = 62.2 \text{ \AA}$ , which agree with our recovered values. Of course, combined inaccuracies in the values of other para-



meters (lifetimes, quantum yields, refractive index, concentrations of acceptor and DPPC, bilayer width) could also account for this result. In any case, even if the  $R_0$  were incorrect, this would only affect the location of the peaks. The shape of the distributions, which is the basis for the above discussion, would remain unchanged.

## 6. Conclusions

Following our recent work on resonance energy transfer (ET) in model membranes (DPPC LUV; ORB as donor, DiIC<sub>1</sub>(7) as acceptor),<sup>12</sup> we measured ET between NBD-PE and Rh-PE in DPPC LUV, both in the gel (25 °C) and fluid (50 °C) phases. These two probes are probably the most used ET pair in bilayer studies.

To obtain more information about both systems, we used global analysis programs for recovery of Gaussian and sum-of-two-Gaussians acceptor concentration distribution functions according to the mean local acceptor concentration formalism.<sup>11,20</sup> Both fluid phase systems could be described by the single Gaussian model with good statistics, even for relatively high acceptor concentrations, for which the discrete model fails. The distributions are wider for the NBD-PE/Rh-PE pair than for the ORB/DiIC<sub>1</sub>(7) pair, indicating lower homogeneity of probe distribution, which is compatible with the studies of self-quenching and concentration depolarization of NBD-PE and the comparison of time-resolved and steady-state ET efficiencies for large concentration of Rh-PE. The gel phase data, however, could not be analyzed with a simple Gaussian model in either system, pointing to strong heterogeneity. Using the statistically successful sum-of-two-Gaussians analysis together with studies of concentration depolarization, self-quenching and comparison of time-resolved and steady-state ET efficiencies, as well as the Monte Carlo simulations of the preceding paper, we propose that that gel phase heterogeneity could result from partial segregation of acceptor into a pseudo (defect) phase and random dispersion of donors in the (bulk) gel lattice for the ORB/DiIC<sub>1</sub>(7) pair, and partial segregation of both donor and acceptor into a pseudo (defect) phase for the NBD-PE/Rh-PE pair. It is concluded that the NBD-PE/Rh-PE can be used in fluid phase membrane studies with caution (molar fraction of NBD-PE  $\leq 0.001$ , molar fraction of Rh-PE  $\leq 0.01$ ) and should not be used for quantitative purposes in gel phase membranes. From this study, we believe that the described analysis method has large potential in detection and characterization of heterogeneity and domains (e.g., gel/fluid) in lipid bilayers.

**Acknowledgment.** This work was supported by PRAXIS XXI (M.C.T., Portugal), Project PRAXIS/P/SAU/14025/1998. L.M.S.L. acknowledges a grant (BD 3927/94) from PRAXIS XXI (Portugal). A.F. acknowledges INVOTAN for financial support. Profs. J. M. G. Martinho and M. N. Berberan-Santos are gratefully acknowledged for a critical reading of the manuscript.

## References and Notes

- (1) Jacobson, K.; Vaz, W. L. C., Eds. *Comments on Molecular and Cellular Biophysics. Vol. 8: Domains in Biological Membranes*; Gordon & Breach: London, 1992.
- (2) Sackmann, E. In *Biophysics*; Hoppe, W., Lohmann, W., Markl, H., Ziegler, H., Eds.; Springer-Verlag: Berlin, 1982; p 425.
- (3) Wang, X. F.; Florine-Casteel, K.; Lemasters, J. J.; Herman, B. J. *Fluoresc.* **1995**, 5, 71.

- (4) Mabrey, S.; Sturtevant, J. M. *Proc. Natl. Acad. Sci. U.S.A.* **1976**, 73, 3862.
- (5) Wolf, D. E.; Maynard, V. M.; McKinnon, C. A.; Melchior, D. L. *Proc. Natl. Acad. Sci. U.S.A.* **1990**, 87, 6893.
- (6) Mendelsohn, R.; Liang, G. L.; Strauss, H. L.; Snyder, R. G. *Biophys. J.* **1995**, 69, 1987.
- (7) Sankaram, M. B.; Marsh, D.; Thompson, T. E. *Biophys. J.* **1992**, 63, 340.
- (8) Davenport, L. *Methods Enzymol.* **1997**, 278, 487.
- (9) Schram, V.; Lin, H.-N.; Thompson, T. E. *Biophys. J.* **1996**, 71, 1811.
- (10) Coelho, F. P.; Vaz, W. L.; Melo, E. *Biophys. J.* **1997**, 72, 1501.
- (11) Loura, L. M. S.; Prieto, M. J. *Phys. Chem. B* **2000**, 104, 6911.
- (12) Loura, L. M. S.; Fedorov, A.; Prieto, M. *Biophys. J.* **1996**, 71, 1823.
- (13) Fontejn, T. A. A.; Engberts, J. B. F. N.; Hoekstra, D. *Biochemistry* **1991**, 30, 5319.
- (14) Connor, J.; Schroit, A. J. *Biochemistry* **1987**, 26, 5099.
- (15) Eastman, S. J.; Wilschut, J.; Cullis, P. R.; Hope, M. J. *Biochim. Biophys. Acta* **1989**, 981, 178.
- (16) Feigenson, G. W. *Biophys. J.* **1997**, 73, 3112.
- (17) Pedersen, S.; Jørgensen, K.; Bækmark, T. R.; Mouritsen, O. G. *Biophys. J.* **1996**, 71, 554.
- (18) Duportail, G.; Merola, F.; Lianos, P. *J. Photochem. Photobiol. A: Chem.* **1995**, 89, 135.
- (19) Lantzsch, G.; Binder, H.; Heerklotz, H. *J. Fluorescence* **1994**, 4, 339.
- (20) Liu, Y. S.; Li, L.; Ni, S.; Winnik, M. A. *Chem. Phys.* **1993**, 177, 579.
- (21) Hope, M. R.; Bally, M. B.; Webb, G.; Cullis, P. R. *Biochim. Biophys. Acta* **1985**, 812, 55–65.
- (22) Arvinte, T.; Cudd, A.; Hildenbrand, K. *Biochim. Biophys. Acta* **1986**, 860, 215.
- (23) McClare, C. W. F. *Anal. Biochem.* **1971**, 39, 527.
- (24) Johansson, L. B. A.; Niemi, A. *J. Phys. Chem.* **1987**, 91, 3020.
- (25) Brackmann, U. *Lamdaochrome Laser Dyes*; Lambda Physik GmbH: Göttingen, Germany, 1986.
- (26) Haugland, R. P. *Handbook of Fluorescent Probes and Research Chemicals*, 6th ed.; Molecular Probes: Eugene, OR, 1996.
- (27) Marquardt, D. W. *J. Soc. Ind. Appl. Math. (SIAM J.)* **1963**, 11, 431.
- (28) Beechem, J. M.; Gratton, E.; Ameloot, M.; Knutson, J. R.; Brand, L. In *Topics in Fluorescence Spectroscopy, Volume 2: Principles*; Lakowicz, J. R., Ed.; Plenum: New York, 1991; 241.
- (29) Coutinho, A.; Prieto, M. J. *Chem. Educ.* **1993**, 70, 425.
- (30) Castanho, M. A. R. B.; Santos, N. C.; Loura, L. M. S. *Eur. Biophys. J.* **1997**, 26, 253.
- (31) Berberan-Santos, M. N.; Prieto, M. J. E. *J. Chem. Soc., Faraday Trans. 2* **1987**, 83, 1391.
- (32) Chattopadhyay, A. *Chem. Phys. Lipids* **1990**, 53, 1.
- (33) Wolf, D. E.; Winiski, A. P.; Ting, A. E.; Bocian, K. M.; Pagano, R. E. *Biochemistry* **1992**, 31, 2865.
- (34) Jabłoński, A. *Bull. Acad. Pol. Sci. Ser. A* **1960**, 8, 259.
- (35) Chen, R.; Bowman, R. L. *Science* **1965**, 147, 729.
- (36) Marsh, D. *Handbook of Lipid Bilayers*; CRC Press: Boca Raton, FL, 1990.
- (37) Medhage, B.; Mukhtar, E.; Kalman, B.; Johansson, L. B.-Å.; Molotkovsky, J. G. *J. Chem. Soc., Faraday Trans.* **1992**, 88, 2845.
- (38) Chattopadhyay, A.; London, E. *Biochemistry* **1987**, 26, 39.
- (39) Snyder, B.; Freire, E. *Biophys. J.* **1982**, 40, 137.
- (40) Prieto, M. J. E.; Castanho, M.; Coutinho, A.; Ortiz, A.; Aranda, F. J.; Gómez-Fernandez, J. C. *Chem. Phys. Lipids* **1994**, 69, 75.
- (41) Fung, B. K.-K.; Stryer, L. *Biochemistry* **1978**, 17, 5241.
- (42) Baumann, J.; Fayer, M. D. *J. Chem. Phys.* **1986**, 85, 4087.
- (43) Massari, S.; Colonna, R.; Folena, E. *Biochim. Biophys. Acta* **1988**, 940, 149.
- (44) Hoekstra, D. *Biochemistry* **1982**, 21, 1055.
- (45) Lakowicz, J. R. *Principles of Fluorescence Spectroscopy*, 2nd ed.; Plenum/Kluwer: New York, 1999.
- (46) Laguiton-Pasquier, H.; Van der Auweraer, M.; De Schryver, F. C. *Langmuir* **1998**, 14, 5172–5183.
- (47) Pevenage, D.; Van der Auweraer, M.; De Schryver, F. C. *Langmuir* **1999**, 15, 8465–8473.
- (48) Derzko, Z.; Jacobson, K. *Biochemistry* **1980**, 19, 6050.
- (49) Schneider, M. B.; Chan, W. K.; Webb, W. W. *Biophys. J.* **1983**, 43, 157.
- (50) Kapitza, H. G.; Rüppel, D. A.; Galla, H. J.; Sackmann, E. *Biophys. J.* **1984**, 45, 577.
- (51) Klausner, R. D.; Wolf, D. E. *Biochemistry* **1980**, 19, 6199.
- (52) Spink, C. H.; Yeager, M. D.; Feigenson, G. W. *Biochim. Biophys. Acta* **1990**, 1023, 25.